An interface-based microscopic model for the failure analysis of masonry structures reinforced with timber retrofit solutions

Fabrizio Greco, Lorenzo Leonetti, Paolo Lonetti, Paolo Nevone Blasi, Arturo Pascuzzo, Giacinto Porco
Department of Civil Engineering, University of Calabria, 87036 Rende (Italy)
fabrizio.greco@unical.it, https://orcid.org/0000-0001-9423-4964
lorenzo.leonetti@unical.it, https://orcid.org/0000-0001-7182-2149
paolo.lonetti@unical.it, https://orcid.org/0000-0003-0678-6860
paolo.nevoneblasi@unical.it., https://orcid.org/0000-0001-8807-2946
arturo.pascuzzo@unical.it, https://orcid.org/0000-0003-3879-6764
giacinto.porco@unical.it, https://orcid.org/0000-0002-9984-5112

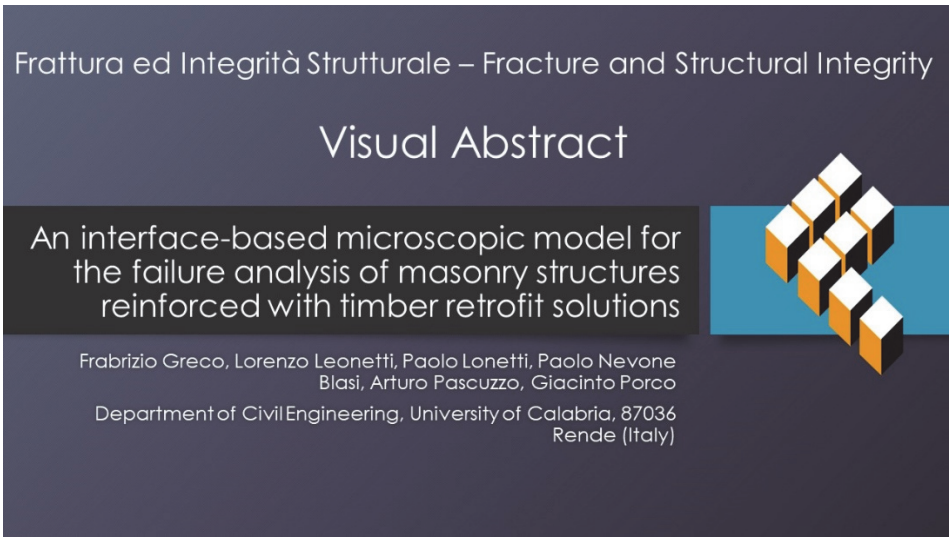

Citation: Greco, F., Leonetti, L., Lonetti, P., Nevone Blasi, P., Pascuzzo, A., Porco, G., An interface-based microscopic model for the failure analysis of masonry structures reinforced with timber retrofit solutions, Frattura ed Integrità Strutturale, 70 (2024) 210-226.

Received: 16.07.2024
Accepted: 19.08.2024
Published: 01.09.2024
Issue: 10.2024

KEYWORDS. Masonry, Crack propagation analysis, Finite elements, Cohesive zone model, Timber, Retrofit, Sustainable solutions.

INTRODUCTION

Over the centuries, masonry has been the primary construction technique for erecting most buildings worldwide [1]. These buildings include monumental edifices with cultural significance, such as churches, castles, noble palaces, and numerous ordinary residential buildings, many of which are currently outdated. The valorization and preservation of cultural heritage constructions, on the one hand, and the recovery and rehabilitation of ordinary buildings, on the other, are now of primary importance in the policies of many countries. Rehabilitating existing residential masonry

buildings is particularly valued for its potential to significantly reduce land consumption, aligning with sustainable urban development goals [2]. Achieving these objectives necessitates a thorough analysis of the structural behavior of masonry under various natural and human-induced actions.

Masonry structures are well known for their excellent performance in withstanding gravitational loads or compressive forces. However, they are highly vulnerable to lateral actions induced by earthquakes. Indeed, even though moderate intensity, lateral forces usually generate dangerous tensile effects on the masonry, compromising the overall structural integrity and causing irreparable damages [3,4]. Therefore, effective retrofitting techniques are essential to enhance the lateral load-bearing capacity of masonry structures. Additionally, proper analysis tools are needed to evaluate the effectiveness of retrofitting techniques by comparing the behavior of the unreinforced masonry (URM) structure with that of the reinforced one.

In recent decades, numerical simulations have become a widely diffused investigation tool to analyze the structural response of masonry structures. Despite extensive research, a general and unified numerical approach allowing a comprehensive structural analysis of masonry structures has not yet been established. Thus, various numerical methods, each with distinct advantages and disadvantages, are currently available. Different ways of classifying numerical methods for analyzing the mechanical behavior of masonry exist (see, for instance, [1,5]). A common and straightforward classification manner consists of grouping numerical methodologies based on the schematization adopted for the masonry in numerical models. According to this classification, one can distinguish Continuous (Macro-models) and Discontinuous (Micro-models) models [6].

Continuous approaches represent masonry as a fictitious anisotropic continuum material, with mechanical properties derived from experimental tests (*i.e.*, phenomenological material properties) or homogenization techniques. These models are computationally efficient and easy to use but less accurate in simulating crack propagation mechanisms. Indeed, smeared crack models are generally employed in continuous approaches. Such damage models tend to diffuse damage over a large area, contrary to the localized nature of the damage that tends to localize in limited regions. This schematization leads to inaccurate predictions of structural capacity and an unlikely representation of the damage zones inside the structure.

Conversely, discontinuous approaches adopt a detailed representation of masonry, considering individual blocks or units and mortar joints. These models accurately reproduce material anisotropy and account for the different mechanical responses of material components and their geometrical arrangement. Additionally, they provide a better simulation of strain localization and damage mechanisms arising in the material components of the masonry. Relevant examples of discontinuous models are those developed in the context of Cohesive Zone Modeling (CZM) approaches [7–9]. Numerical models based on CZM are generally classified into simplified [1,6,10] or detailed [11–13] schemes depending on how the mortar joint is represented. In particular, in simplified modeling schemes, mortar joints are not explicitly represented, and the masonry consists of expanded bricks (or units) that are mutually connected through interface elements. This approach enhances computational efficiency without sacrificing numerical reliability.

The literature reports various retrofitting techniques for URM to improve its earthquake resistance, including (*i*) surface treatment, (*ii*) stitching and grout/epoxy injection, (*iii*) external reinforcement, (*iv*) confinement of the masonry, and (*v*) mesh reinforcement. In particular, the external reinforcement technique involves installing an auxiliary structural system next to the URM. This system offers the advantage of enhancing the mechanical performance of the masonry while preserving its authenticity. Besides, in some cases, it is entirely reversible. Traditionally, materials used for this technique include steel, titanium, and fiber-reinforced polymers [14]. More recently, there has been growing interest in using eco-friendly materials such as bamboo, wood, and natural fiber-based composites [15], driven by global sustainability requirements imposed by governments worldwide. In this framework, several studies have evaluated timber-based retrofitting solutions for URM buildings. For instance, Damiani et al. [16] have developed a retrofit system based on vertical timber posts and horizontal nogging nailed by oriented timber-based sheets (OSB panels) anchored to the URM through several distributed steel plates, proposing a step-by-step design procedure based on analytical equations. The validity of the retrofit system and the associated design analytical equations have been next assessed experimentally by Guerrini et al. [17]. In addition, Guerrini et al. [18] have conducted numerical simulations on the experimental study cases of Damiani et al. [16]. In particular, to reproduce the mechanical response of the masonry, they have used the commercially available software TREMURI [19], which employs an equivalent-frame formulation using nonlinear macroelements. Busselli et al. [20] have investigated numerically the behavior of a retrofit system consisting of timber-based products (panels and strong-backs) fixed to the masonry walls from both structural and energetic viewpoints. In particular, the structural behavior of the masonry has been modeled using an equivalent, homogeneous, and isotropic material whose nonlinear behavior due to damage has been reproduced using a Concrete Damage Plasticity model [21]. Collectively, the previous studies indicate that the retrofitting system of URM based on the use of timber frame structures represents a promising technique to be applied to existing masonry buildings. For this reason, further investigations on the topic are needed to advance the knowledge further. Numerical models capable of accurately reproducing all masonry failure mechanisms are essential to achieve these goals.

The main aim of this paper is to propose a refined numerical modeling strategy for analyzing the in-plane failure behavior of URM structures reinforced with timber-based retrofit solutions. The proposed model is developed in a two-dimensional Finite Element setting, in which the masonry is modeled using linear elastic plane stress finite elements and zero-thickness interface elements. Specifically, masonry consists of expanded brick units mutually jointed by zero-thickness cohesive interface elements that reproduce the nonlinear behavior of masonry because of the failure mechanisms of the mortar joints. Besides, the external reinforced system consists of braced timber frame structures modeled by elastic brittle truss elements. The interaction between the URM and the reinforced timber frame system is reproduced using kinematic constraint conditions that reproduce the behavior of mechanical anchorage connections. The validity of the proposed model regarding the failure behavior of URM structures has been validated through comparison results with a relevant benchmark case for which experimental and numerical results are available in the literature. Subsequently, the efficacy of the proposed retrofitting strategy has been assessed by performing nonlinear incremental static analysis (pushover analysis) on single masonry panels and a two-story masonry wall.
This paper consists of four sections. Following the introduction, the first section comprehensively describes the theoretical aspect and numerical implementation of the proposed numerical model. Then, numerical results are presented and discussed. Finally, the main conclusions of the work are outlined in the conclusion section.

THEORETICAL FORMULATION AND IMPLEMENTATION DETAILS

This section provides the theoretical background and the main numerical implementation details of the proposed model, with particular attention devoted to the three different sub-models that form the present numerical approach.

Cohesive zone-based micromechanical model for regular masonry

Regular masonry is modeled as a heterogeneous material having two phases, *i.e.*, the units and the joints, arranged according to a periodic microstructure. The units are regarded as made of a linearly elastic material, whereas the joints are represented as damageable zero-thickness interfaces equipped with a cohesive-type traction-separation law. Such modeling is known in the technical literature as the so-called simplified microscopic approach for masonry instead of detailed microscopic ones, where joints are modeled as a continuous elastic phase placed between the units [1].
The theoretical formulation for finite element-based modeling of masonry relies on the two-phase representation of masonry depicted in Fig. 1-a, with reference to the planar setting, since only the in-plane failure behavior is considered in the present work.

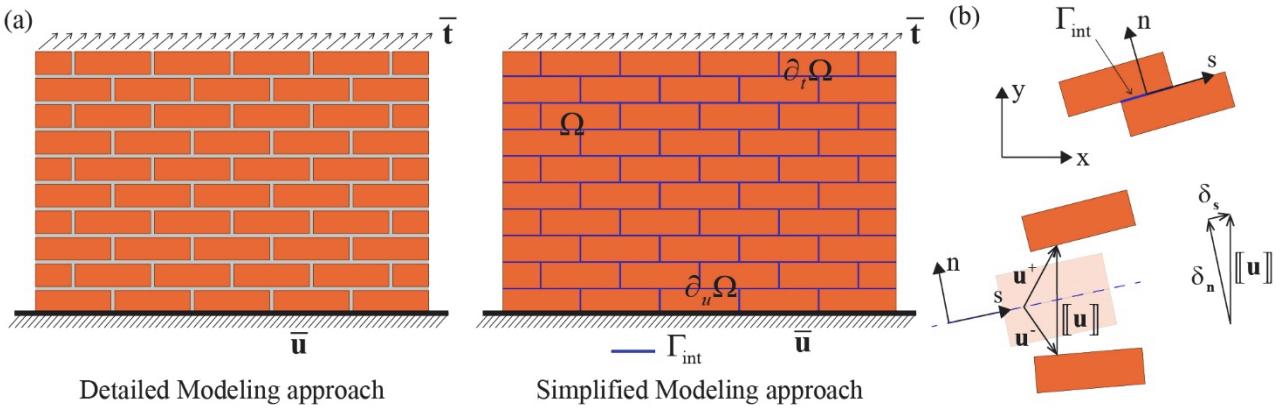

Figure 1: (a) An in-plane masonry structure: a comparison between detailed and simplified modeling approaches (b) Local system of coordinates along a cohesive boundary and associated displacement jump components.

Let $\Omega \subset R^2$ be the region occupied by the given masonry structure, whose external boundary $\partial\Omega$ consists of two disjoint portions $\partial_t\Omega$ and $\partial_u\Omega \neq \varnothing$, where traction and displacement boundary conditions are prescribed (see Fig. 1-a). Moreover, this structure contains several interfaces embedded between the units, which are collectively denoted as Γ_{int}. The units behave elastically, whereas the interfaces are equipped with a cohesive traction-separation law of mixed-mode type, with the aim of reproducing multiple crack onset and propagation phenomena under general loading conditions.

Under the common assumptions of small displacements, quasi-static loading, and negligible volume forces, the mechanical problem of such a composite system can be mathematically expressed by a nonlinear boundary value problem (BVP) stated in the following weak form, *i.e.,* find $\boldsymbol{u}$ such that:

$$\int_{\Omega\setminus\Gamma_{\text{int}}} \boldsymbol{\sigma} : \nabla \delta\boldsymbol{u} \, \mathrm{d}\Omega + \int_{\Gamma_{\text{int}}} \boldsymbol{t}_{\text{int}}\left([[\boldsymbol{u}]], d\right) \cdot [[\delta\boldsymbol{u}]] \, \mathrm{d}\Gamma = \int_{\partial_t\Omega} \overline{\boldsymbol{t}} \cdot \delta\boldsymbol{u} \, \mathrm{d}\Gamma \qquad \forall \delta\boldsymbol{u} \tag{1}$$

In Eqn. (1), $\boldsymbol{u}$ is the unknown displacement field and $\delta\boldsymbol{u}$ its arbitrary kinematically admissible variation, $\Omega\setminus\Gamma_{\text{int}}$ collectively denotes the subdomains corresponding to the discontinuous phase, *i.e.*, the units, $\boldsymbol{\sigma} = \boldsymbol{C} : \nabla_s \boldsymbol{u}$ is the stress tensor, being related to the infinitesimal strain tensor $\boldsymbol{\varepsilon} = \nabla_s \boldsymbol{u}$ through the linearly elastic constitutive tensor $\boldsymbol{C}$, $\overline{\boldsymbol{t}}$ is the surface traction applied over $\partial_t\Omega$, $\boldsymbol{t}_{\text{int}} = \boldsymbol{t}_{\text{int}}^-$ is the cohesive traction vector, being defined over the negative side of the embedded interfaces, $[[\boldsymbol{u}]] = \boldsymbol{u}^+ - \boldsymbol{u}^-$ is the displacement jump between the two sides of the interfaces and $[[\delta\boldsymbol{u}]]$ is its arbitrary variation, and $d \in [0,1]$ denotes a (scalar) history variable, which physically represent the damage state of the cohesive interfaces.
In particular, the following coupled mixed-mode traction-separation law is assumed for the cohesive interfaces:

$$\boldsymbol{t}_{\text{int}}\left([[\boldsymbol{u}]], d\right) = (1-d)\boldsymbol{K}[[\boldsymbol{u}]] \tag{2}$$

where $\boldsymbol{K}$ is the second-order interface stiffness tensor, representing the initially elastic behavior of undamaged interfaces. The constitutive law expressed by means of Eqn. (2) can be rewritten in the following matrix form, after a suitable local coordinate system attached to each interface is defined:

$$\begin{bmatrix} t_n \\ t_s \end{bmatrix} = (1-d)\begin{bmatrix} K_n & 0 \\ 0 & K_s \end{bmatrix}\begin{bmatrix} \delta_n \\ \delta_s \end{bmatrix} \tag{3}$$

where the subscripts s and n refer to local components with respect to the tangential and normal directions, respectively. In particular, $t_s = \boldsymbol{t}_{\text{int}} \cdot \boldsymbol{s}$ and $t_n = \boldsymbol{t}_{\text{int}} \cdot \boldsymbol{n}$, and, accordingly, $\delta_s = [[\boldsymbol{u}]] \cdot \boldsymbol{s}$ and $\delta_n = [[\boldsymbol{u}]] \cdot \boldsymbol{n}$, where $\boldsymbol{s}$ and $\boldsymbol{n} = \boldsymbol{n}^-$ are the tangent and outer normal unit vectors referring to the negative side of the interface. Moreover, in the absence of coupling stiffness terms between these directions, K_n and K_s are the normal and tangential interface stiffness coefficients, which can be obtained from the elastic properties of masonry components (*i.e.*, Young's moduli E_u, E_j and shear moduli G_u, G_j of units and joints) as well as from the joint thickness h_j, according to the relations adopted in REF. [1]:

$$K_n = \frac{E_u E_j}{h_j\left(E_u - E_j\right)}, \qquad K_s = \frac{G_u G_j}{h_j\left(G_u - G_j\right)} \tag{4}$$

The damage variable d is defined by the following expression:

$$d = \begin{cases} 0 & \text{if } \delta_{\max} < \delta_0 \\ 1 - \dfrac{\delta_0}{\delta_{\max}} \exp\left(-2\dfrac{\delta_{\max} - \delta_0}{\frac{2G_f}{f_t} - \delta_0}\right) & \text{if } \delta_{\max} \geq \delta_0 \end{cases} \tag{5}$$

and strictly depends on the largest value $\delta_{\max}$ ever attained by the equivalent displacement jump δ, the latter being defined based on the following interface version of a capped Drucker-Prager criterion, originally proposed in [6]:

$$\delta = \begin{cases} AI_\delta + BJ_\delta & \text{if } J_\delta \geq \dfrac{A-C}{D-B} I_\delta \\ CI_\delta + DJ_\delta & \text{if } J_\delta < \dfrac{A-C}{D-B} I_\delta \end{cases} \tag{6}$$

In Eqn. (6), I_δ and J_δ have the following definitions:

$$I_\delta = \left(1+\nu_j\right)\delta_n, \quad J_\delta = \frac{1}{1+\nu_j}\sqrt{\frac{1+\nu_j+\nu_j^3+\nu_j^4}{3}\delta_n^2 + \frac{1}{4}\delta_s^2} \tag{7}$$

both depending on the Poisson's ratio ν_j of masonry joints, whereas the constants A, B, C, D are functions of the main strength parameters of masonry joints, i.e., the uniaxial tensile strength f_t, the uniaxial compressive strength f_c, and the biaxial compressive strength f_b:

$$A = \frac{1}{2}\frac{f_c - f_t}{f_c}, \quad B = \frac{\sqrt{3}}{2}\frac{f_c + f_t}{f_c}, \quad C = \frac{\left(f_b - f_c\right) f_t}{f_b f_c}, \quad D = \sqrt{3}\frac{\left(2f_b - f_c\right) f_t}{f_b f_c} \tag{8}$$

It is worth noting that such a composite criterion can account for the competition between different failure mechanisms in masonry structures, including the shear-tension and the shear-compression failure modes (being strictly related to the cohesive-frictional properties of masonry joints), as well as the masonry crushing under compressive loads, which is represented by the additional compressive cap to the constitutive model of joints.

Truss model for timber frame-based retrofitting system

The newly proposed timber frame-based solution for the in-plane strengthening of masonry structures is similar to that recently investigated in REF. [16], which is made of vertical timber posts, horizontal nogging elements, top and bottom timber sill plates, and oriented-strand board (OSB) panels. Both systems are conceived to be fastened to the interior of masonry piers and spandrels, but the present one replaces the OSB panels with diagonal braces as the main difference.

In the proposed retrofitting system, the in-plane flexural strength is entrusted to the resulting timber frame composed of posts, nogging elements, and sill plates, whereas the diagonal bracing system assures the in-plane shear strength. The resulting system consists of multiple modular braced frames kinked to each other by means of steel connections. The typical geometric configuration of a retrofit module made of timber elements is reported in Fig. 2. Special frames with variable shapes and dimensions could also be used to accommodate geometric constraints, like in the presence of pitched roofs or misaligned openings in the masonry walls.

The retrofit system analyzed in the present work is modeled as a planar truss, meaning that horizontal, vertical, or diagonal timber members are represented by single (1D) bar elements. Such finite elements are equipped with a linear elastic-brittle damage constitutive behavior to simulate the sudden failure of timber elements under tensile loading. In practice, the bar elongation ε is related to the axial force N through the following relation:

$$N = k_a\left(\varepsilon_{\max}\right)\varepsilon \qquad k_a\left(\varepsilon_{\max}\right) = \begin{cases} EA & \varepsilon_{\max} < \varepsilon_0 \\ \kappa EA & \varepsilon_{\max} \geq \varepsilon_0 \end{cases} \tag{9}$$

where k_a is the axial stiffness of bar elements, E is the longitudinal Young's modulus of undamaged timber, A denotes the element cross-section, $\varepsilon_{\max}$ represents the maximum elongation measured over the entire deformation history, $\varepsilon_0 = f_0/E$ is the elastic limit for the bar elongation (f_0 being the longitudinal tensile strength of timber), and κ is a minimal value, corresponding to the residual axial stiffness of the failed timber element. In the present work, it is assumed $\kappa = 1\times10^{-5}$. Furthermore, all the mutual connections between the timber members are hinges.

The above assumptions are coherent with the nature of usual steel connections found in timber structures, which are not able to transfer significant bending moments. Finally, as usually done for bracing systems in frame structures, compressed

diagonal members are supposed to be kept inactive from the beginning of simulations due to the occurrence of buckling phenomena.

Modeling of interaction between masonry and timber frame

The overall performance of the adopted timber frame-based retrofitting solution is highly influenced by the quality of its connections with the existing masonry walls. These connections are placed at the corners of the attached timber frames, as sketched in Fig. 2, and can be realized through chemical or mechanical anchors at the interior side of masonry walls.
In the present work, the timber frame-to-masonry connections are modeled using nonlinear deformable links equipped with an elastic-brittle behavior to potentially simulate the connection failure. Specifically, the following constitutive law is assumed:

$$\begin{Bmatrix} F_x \\ F_y \end{Bmatrix} = \begin{bmatrix} k(\eta_{\max}) & 0 \\ 0 & k(\eta_{\max}) \end{bmatrix} \begin{Bmatrix} \eta_x \\ \eta_y \end{Bmatrix} \qquad k(\eta_{\max}) = \begin{cases} k_0 & \eta_{\max} < \eta_0 \\ \xi k_0 & \eta_{\max} \geq \eta_0 \end{cases} \tag{10}$$

where F_x and F_y are the horizontal and vertical forces transferred by the anchor, η_x and η_y are the horizontal and vertical degrees of freedom of the deformable link, $\eta = \sqrt{\eta_x^2 + \eta_y^2}$ and $\eta_{\max}$ represent the relative displacement between frame and masonry at the anchor location and its maximum values measured over the entire loading history, k_0 is the initial stiffness of undamaged connection, $\eta_0 = F_0 / k_0$ is the elastic limit for the relative displacement (F_0 being the connection strength for the assumed isotropic behavior), and ξ is a very small value (here fixed equal to 1×10^{-5}), corresponding to the residual stiffness of the failed connection.

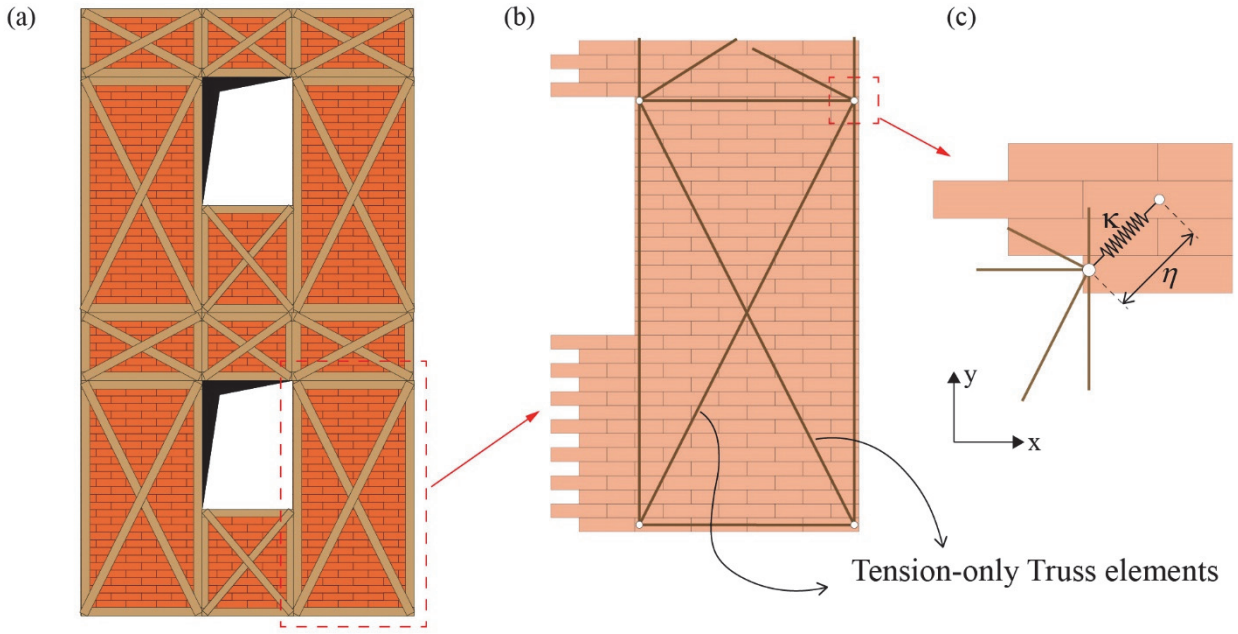

Figure 2: (a) A schematic of the retrofitting system based on timber frames with diagonal bracings; (b) A depiction of the numerical schematization; (c) Numerical schematization of the timber frame-to-masonry connection.

NUMERICAL RESULTS

This section presents numerical results to assess the efficacy of the proposed retrofitting strategy for URM structures using timber-based retrofit solutions. Specifically, two study cases are investigated. The first case involves a masonry panel with an opening subjected to shear force, initially investigated experimentally by Vermeltfoort et al. [22]. This case serves as a relevant benchmark for assessing the reliability of the interface-based cohesive model described in the

section on theoretical formulation and numerical implementation. The second case consists of a two-story masonry wall with openings, representing a common wall of a real-life two-story masonry building. This case is significant for evaluating the practical application and effectiveness of the proposed retrofitting strategy.

A shear test of a masonry wall with an opening

Fig. 3-a shows a masonry wall with a length of 900 mm and a height of 1116 mm, subjected to a vertical and uniform pressure p=0.30 MPa and an increasing shear force F. The wall structure consists of solid clay bricks, each measuring 210 mm in length, 52 mm in height, and 100 mm in width, joined by 10 mm thick mortar joints. This case was experimentally investigated by Vermeltfoort et al. [22], who provided comprehensive information on the mechanical properties of material constituents and the structural response of the wall. In particular, the experimental results corresponding to the shear test of the wall are expressed as horizontal displacement (δ) versus force (F) curves and the associated failure modes. The results of Vermeltfoort et al. have served as a benchmark case for many researchers who have developed numerical models to reproduce the mechanical behavior of masonry structures. Therefore, in the present study, the shear test of Vermeltfoort et al. has been used to validate the reliability of the proposed model. The Young's Modulus and Poisson's ratio of brick units and the mortar are assumed to be E_b=16700 MPa and ν_b=0.15, and E_m=782 MPa and ν_m=0.14, respectively. The normal and shear elastic stiffnesses of cohesive interface elements are defined according to Eqs. (4).

Fig. 3-b shows the computational mesh adopted in numerical simulations. In this schematization, cohesive interface elements, placed along all the boundaries of the bulk elements representing the brick units, have been discretized through line segments of a constant size of 0.003 m (see the zoomed view of Fig. 3-b). Additionally, the two-dimensional domains corresponding to the brick units are discretized using plane stress finite elements arranged according to unstructured schematizations generated using a Delaunay-type triangulation algorithm.

Fig. 4 compares the prediction of the proposed model with experimental results achieved by Vermeltfoort et al. [22] and numerical results from Vandoren et al. [6], Lourenço and Rots [23], D'Altri et al. [24], and Milani [25]. The results indicate that the proposed method is in line with both experimental and numerical data. Specifically, the peak load predicted by the proposed method agrees very well with the experimental peak load and that predicted by Milani. Additionally, the post-peak softening curve aligns with those from other numerical models. Thus, it can be concluded that the proposed method is a robust and reliable tool for predicting the failure behavior of masonry structures.

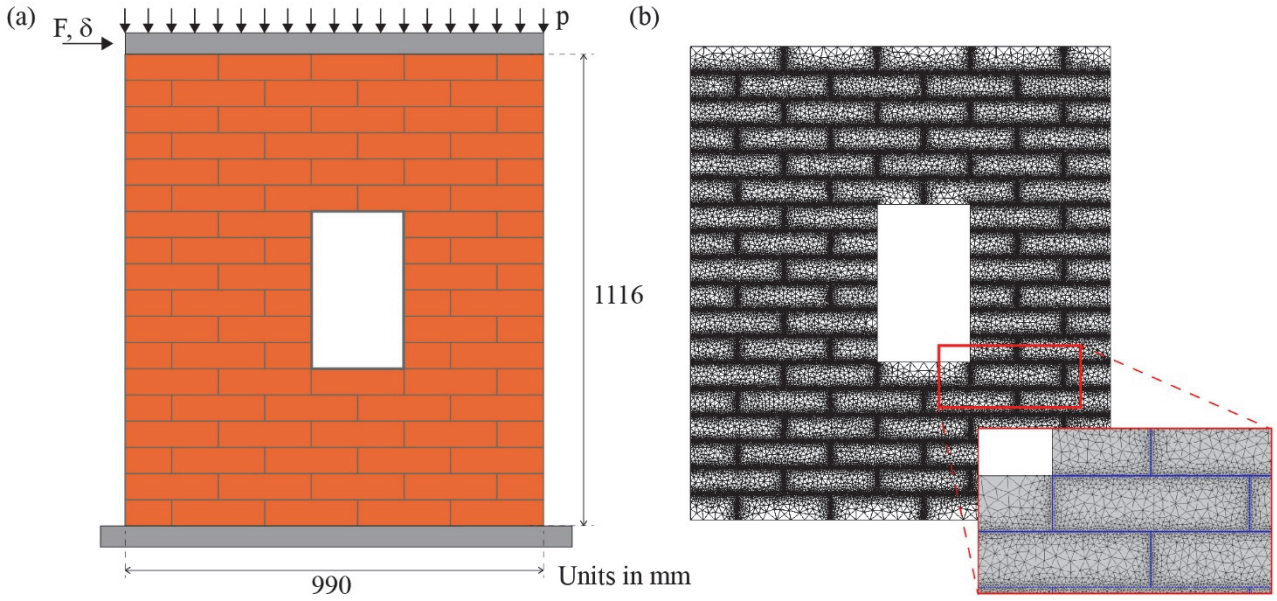

Figure 3: A masonry wall with an opening. (a) geometry and boundary conditions. (b) a depiction of the computational mesh.

The validated numerical model has been used to assess the efficacy of the proposed retrofitting strategy based on a timber frame sub-structure. Specifically, timber frame structures with cross braces elements are attached to the masonry wall. The timber frame elements consist of square-section wooden beams with side Lt, made of hardwood with Young's modulus and yield stress equal to E_t=9000 MPa and σ_t=10 MPa, respectively. Fig. 5-a illustrates the geometrical arrangement of the masonry wall retrofitted by the timber frame system, whereas Fig. 5-b shows the computational mesh adopted in numerical

simulations. Notably, the mechanical connections between these structures are assumed to be undamageable, meaning that the failure of the entire system can occur due to the failure of either the masonry wall or the timber frame structure.

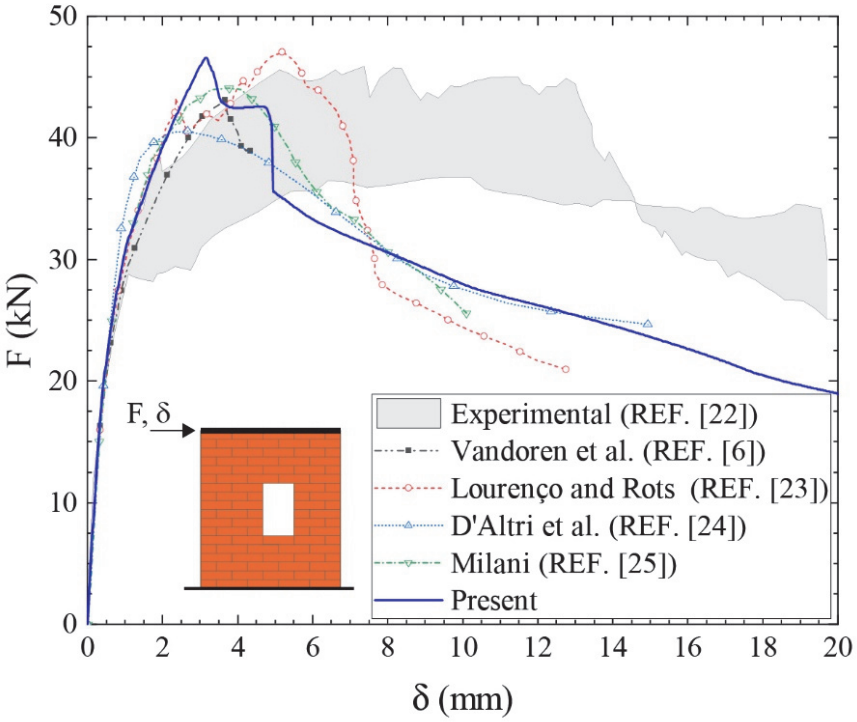

Figure 4: A masonry wall with an opening: Validation.

Fig. 6-a shows the load (F) versus horizontal displacement (δ) curve for three retrofitting systems with the same layout but different cross-sectional dimensions of the timber frame trusses (L_t). The graph also includes the curve for the unreinforced masonry (URM) case for comparison. The results indicate that the proposed retrofit system significantly enhances the bearing capacity of the URM wall against lateral actions, with the peak load increasing as the timber frame cross-section grows. Specifically, the peak load achieved for L_t=50 mm, 75 mm, and 100 mm is higher than that of the URM case of 5.90%, 66.55%, and 139.50%, respectively. Examining the post-peak behavior of the retrofitted cases reveals that the curves are characterized by two consecutive sudden drops in the resistance. To explain this behavior, the case with L_t = 75 mm is considered, and the structural response of the timber frame elements is investigated in detail. The trend of the load-displacement curve for this case can be subdivided into three regions, denoted by Roman numerals in the graph.

Fig. 6-b illustrates the structural configurations corresponding to these regions. Note that only diagonal bracing members in tension are depicted. It can be observed that each drop in the post-peak curve is associated with the sudden rupture of a diagonal bracing member in the timber frame retrofit system. Such rupture leads to a significant loss of the bearing capacity of the retrofitted wall. Regardless of the dimensions of the timber frame elements, once both the bottom diagonal elements broke, the bearing capacity of the structure becomes 8% lower than that of the URM wall. Then, despite the brittle behavior experienced by the retrofitted wall, the rupture of the retrofit system does not cause capacity losses considerably different than the URM wall, thus highlighting that the proposed retrofitting strategy does not involve sudden collapses of the entire wall.

Additional results in terms of damage distribution within interface elements are depicted in Fig. 7. This figure shows the extent and intensity of the damage for the examined cases corresponding to two levels of the external force, which are indicated as F_{URM}^{MAX} and $F_{URM}^{MAX}/2$, where F_{URM}^{MAX} represents the peak load obtained for the URM wall.

The results show that the retrofitting system mitigates the extent and intensity of damage within the interface elements. Specifically, this beneficial effect becomes more pronounced as the dimensions of the timber frame components increase, underscoring the significant enhancement in bearing capacity offered by the proposed retrofitting strategy.

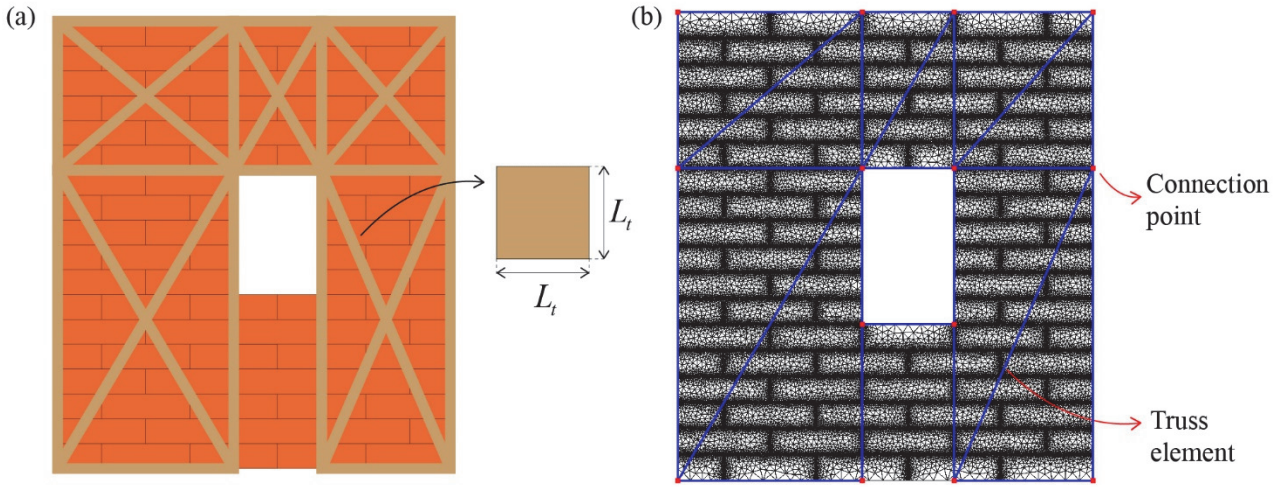

Figure 5: A masonry wall with an opening: (a) A schematic of the retrofitting scheme. (b) Computational mesh.

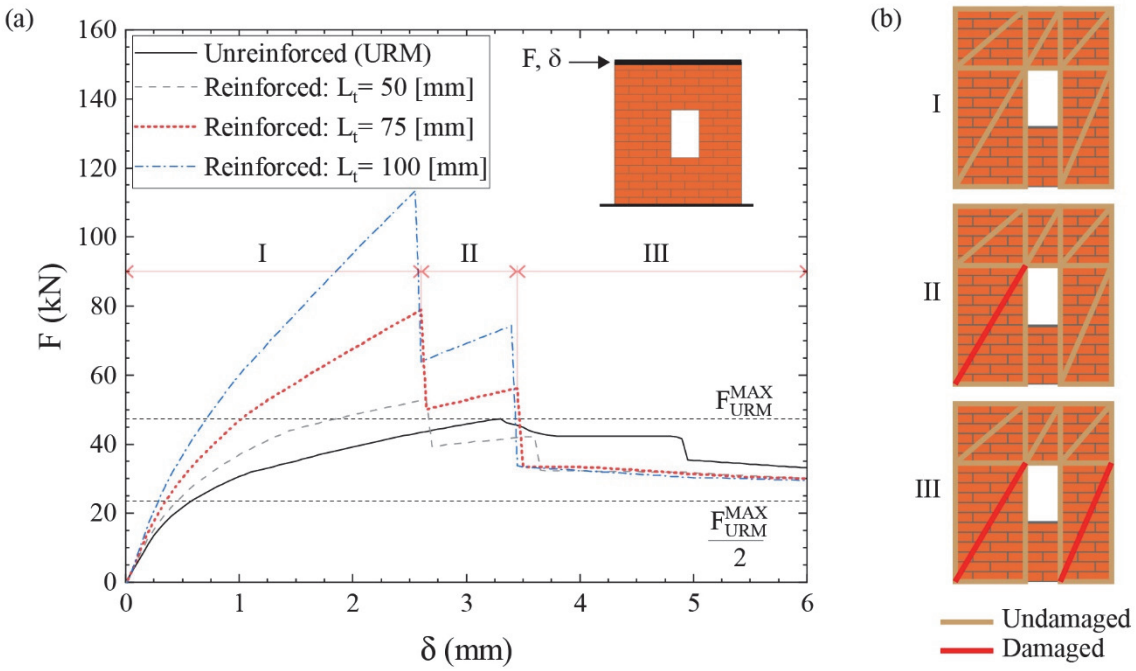

Figure 6: A masonry wall with an opening: (a) Load versus displacement curves of URM wall reinforced by retrofitted scheme depicted in Fig. 5. (b) Snapshots of the configurations of the reinforced masonry wall with L_t = 75 mm relative to the horizontal displacement values marked by Roman numerals.

Further analyses are developed to investigate the effects induced by different geometrical configurations of the timber frame retrofit system. Fig. 8 illustrates three configurations of the timber frame system used to retrofit the masonry wall. In particular, the first scheme corresponds to the one previously discussed, while the second and third represent potential alternative arrangements. All schemes are assumed to feature the same dimensions for the structural frame, with L_t = 75 mm. Fig. 9 compares the load versus displacement curves corresponding to the three retrofit schemes and the unreinforced wall. The results demonstrate an enhancement in the load-bearing capacity of the panel across all investigated cases. However, the behaviors differ significantly. Specifically, the RS2 notably increases the peak load by approximately 137% compared to URM. Nevertheless, this configuration exhibits a marked brittle behavior for the wall once the maximum load is reached because a sudden collapse in the overall load-bearing capacity is observed. As highlighted in Fig. 10, this behavior can be attributed to the sudden failure of the upper diagonal elements of the retrofit system.

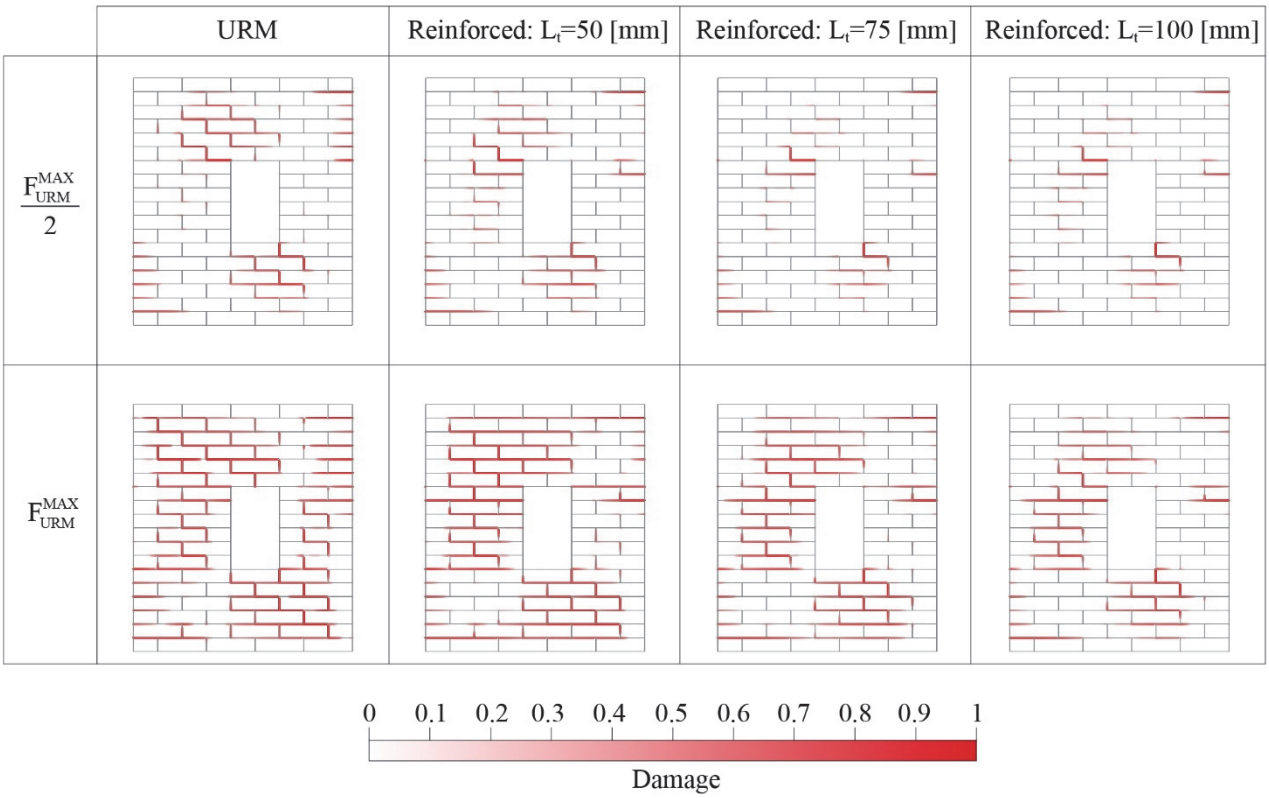

Figure 7: A masonry wall with an opening: Maps of the damage within the interface elements for levels of the external force equal to the maximum and half the maximum force of the URM wall.

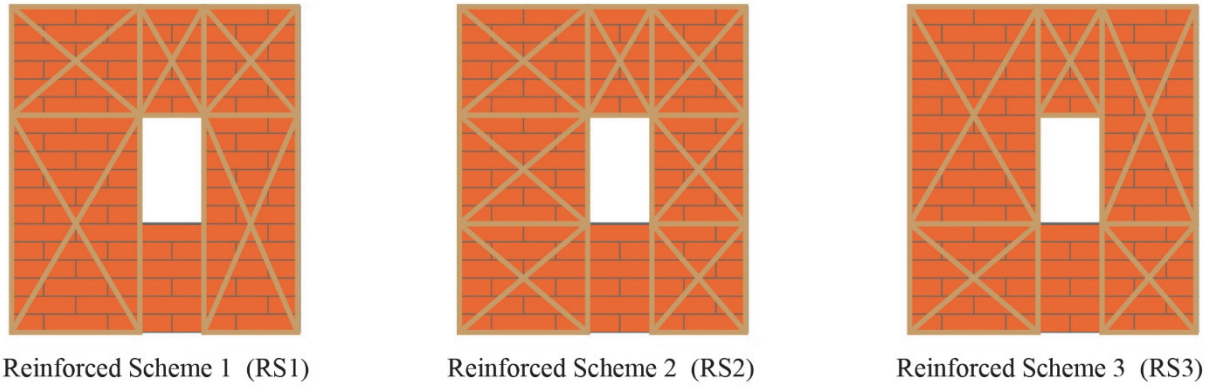

Figure 8: A masonry wall with an opening: Comparison in terms of geometrical arrangement of timber frame retrofit system.

The RS3 enhances the bearing capacity of the wall by about 59% compared to URM. Similar to RS2, it exhibits a brittle behavior after reaching the maximum load force. The abrupt breakage of the diagonal bracing elements in the upper frames is responsible for this behavior. From these results, it transpires that the retrofitting system should be configured in such a way as to avoid the simultaneous failure of multiple bracing elements. Such an aspect can properly prevent the retrofitting frame from inducing brittle failure mechanisms in the wall that can lead to its sudden collapse.

Alternatively, an effective strategy to prevent the retrofitting system from causing brittle behavior in the masonry structure could involve increasing the number of bracing elements, thereby enhancing the redundancy of the timber frame sub-structure. With this strategy, the sudden loss of a single bracing element would not generate impulse forces capable of triggering the collapse of the entire structure. Instead, the load previously carried by the failed element would be redistributed among the remaining intact components, each experiencing only a slight increase in internal stress.

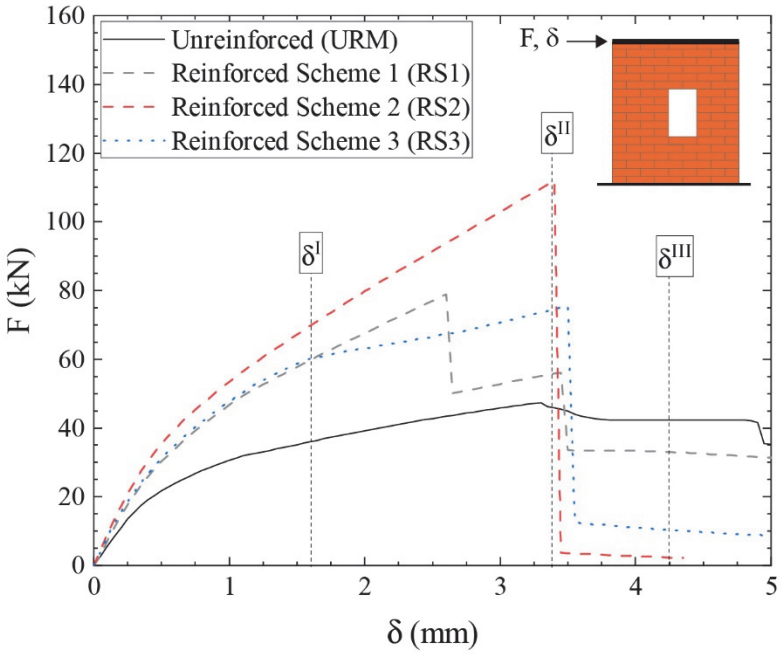

Figure 9: A masonry wall with an opening: Comparison in terms of geometrical configuration of timber frame retrofit system.

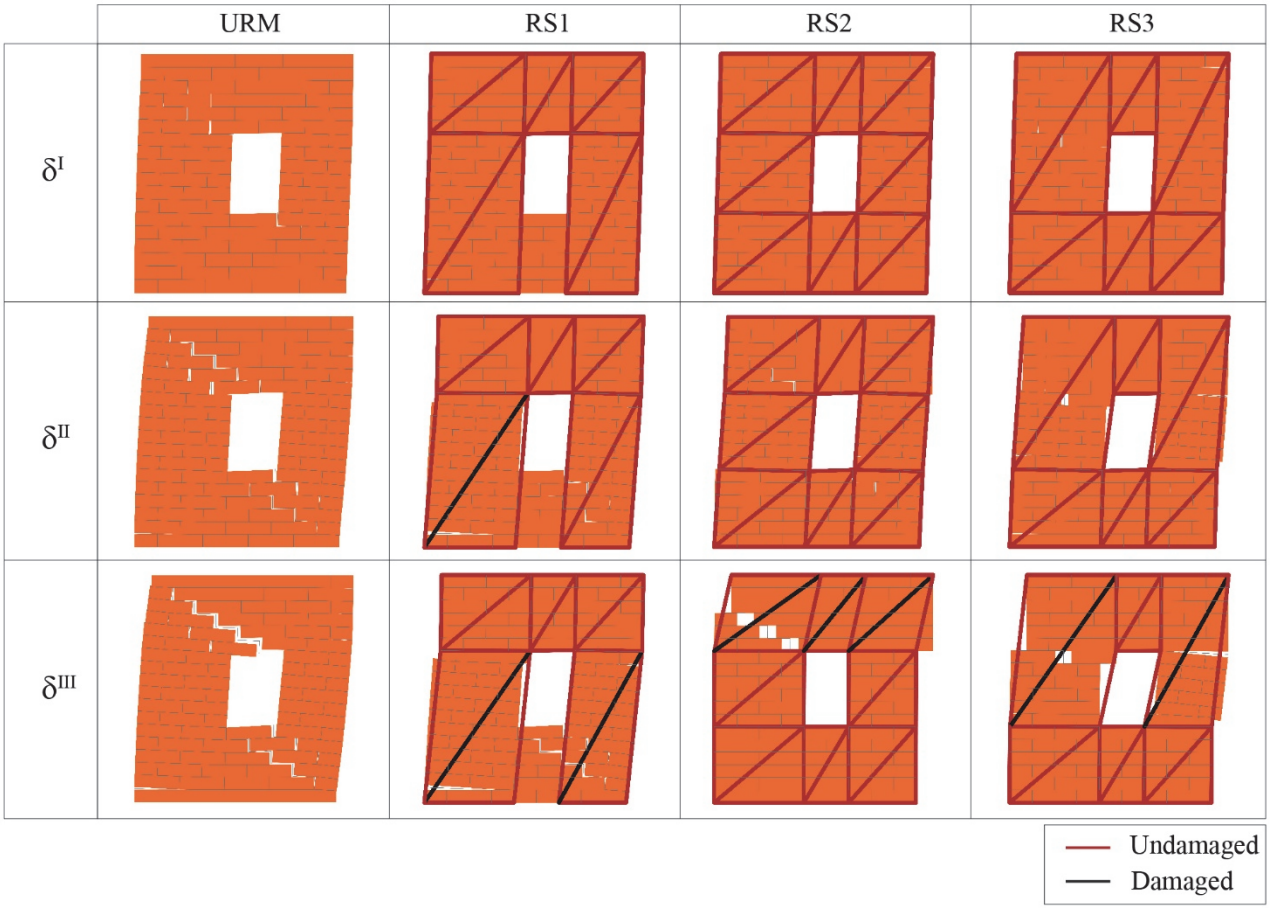

Figure 10: A masonry wall with an opening: Snapshots of the deformed configurations of the masonry walls relative to the horizontal displacement values marked by the symbols δ^{I}, δ^{II}, and δ^{III} in Fig. 9.

Analysis of a two-story masonry wall

Fig. 11-a depicts a two-story masonry wall measuring 3960 mm in length and 3472 mm in height, featuring four openings regularly spaced. This configuration is typical of real-life masonry buildings, making it a valuable case study to evaluate the effectiveness of the proposed retrofitting strategy using timber frame structures. The masonry is assumed to be identical to that investigated in the previous section. Therefore, it consists of solid clay bricks of 210 mm x 52 mm x 100 mm, jointed by mortar joints of 10 mm in thickness. The Young's Modulus and Poisson's ratio of brick and mortar are E_b=16700 MPa and ν_b=0.15, and E_m=782 MPa and ν_m=0.14, respectively.

Like the previous case of study, the numerical model involves linear elastic expanded bricks connected through zero-thickness interface elements for which elastic stiffnesses are evaluated using Eqs (4).

Fig. 11-b depicts the computational mesh employed in numerical simulations. The interface elements placed along all the boundaries of brick units have been discretized using line elements of 6 mm in length, whereas the mesh of the brick units consists of triangular plane stress elements, whose maximum size is equal to 18 mm.

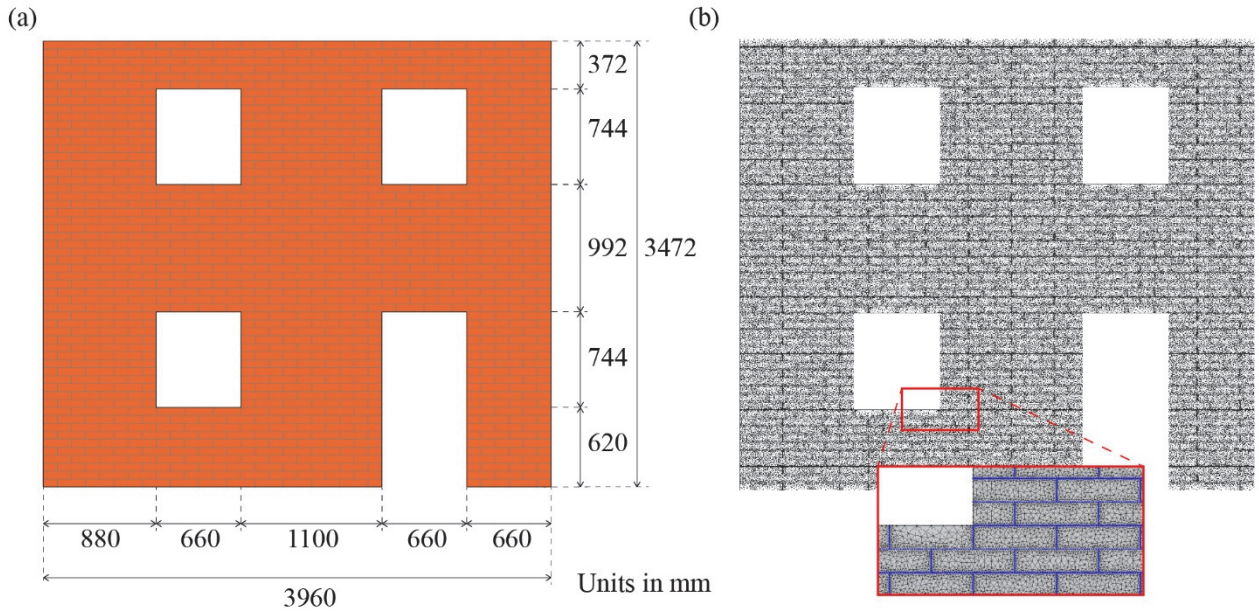

Figure 11: A two-story masonry wall: (a) a schematic of the geometry. (b) a depiction of the computational mesh.

Fig. 12-a presents a schematic representation of the kinematic and loading conditions applied to the wall in the numerical simulations. The model incorporates rigid connector kinematic constraints to account for the presence of horizontal slabs positioned at heights of 1.736 m and 3.472 m. Additionally, the wall is fixed at the base. In the proposed study, the behavior of the wall is investigated through a pushover analysis using twofold loading patterns: the first consists of constant vertical loads applied at the heights of the slabs and equal to p=5.4x10^5 N/m, while the second comprises increasing horizontal forces arranged according to a triangular pattern. The monitored displacement is the horizontal displacement of the upper slab at a height of 3472 mm. Fig. 12-b shows the pushover curve of the wall, expressed in the form of horizontal displacement (δ) and horizontal force (F). Figs. 13-a and 13-b illustrate the map of damage inside interface elements and snapshots of the deformed configuration of the wall occurring at horizontal displacement values (δ) marked in Fig. 12-b by Roman numerals, respectively.

The results denote that the wall initially exhibits a linear elastic behavior up to δ=1.2 mm, followed by a nonlinear response in which a peak load of 76.2 kN at δ=4.9 mm is reached. Subsequently, the wall enters a softening phase, progressively losing its bearing capacity. Examining the damage maps reported in Fig. 13-a reveals that the wall collapses because of the occurrence of tensile regions localized in the bottom part. More precisely, the collapse is triggered by a diagonal shear failure mechanism developing across the left opening (see Fig. 13-b). Additionally, the right pier is subjected to a combined compressive and shear action, which leads to the detachment of the vertical mortar joints in the central region of the pier.

The proposed retrofitting strategy is now applied to retrofit the masonry wall. In particular, two reinforcement schemes are considered (see Fig. 14): the first scheme (denoted as RS1) entails placing the reinforcement only on the first level of the wall, while the second scheme (named RS2) reinforces the entire wall. In both cases, the timber frames consist of square beams with a side L_t=75 mm, having Young's modulus and yield strength equal to 9000 MPa and 10 MPa, respectively.

Notably, the timber frame for the right pier of the wall at the first level is configured based on the findings from Fig. 13. More precisely, multiple bracing elements are introduced in the frame to mitigate the expansion effect of the masonry caused by the crisis of the vertical mortar joints.

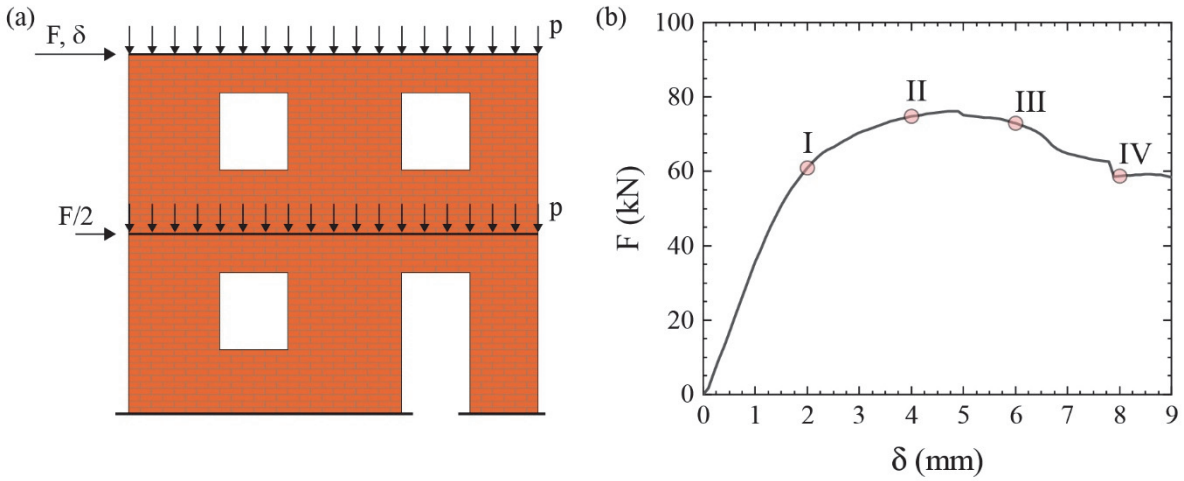

Figure 12: A two-story masonry wall: (a) boundary conditions, (b) Load vs displacement curve.

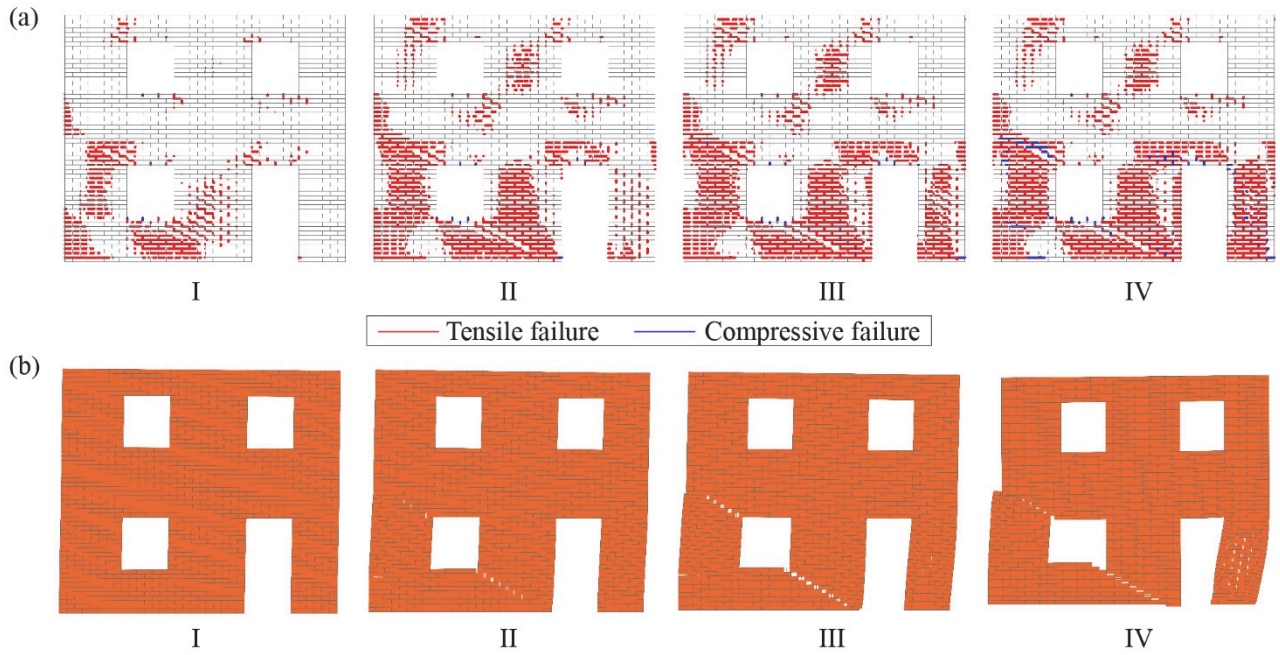

Figure 13: A two-story masonry wall: (a) Map of the damage inside interface elements (b) Snapshots of the deformed configurations of the masonry wall relative to the horizontal displacement values marked by Roman numerals in Fig. 12-b.

Fig. 15 compares the pushover curves associated with the unreinforced wall with those obtained for the two reinforced schemes reported in Fig. 14. The results show that both reinforced schemes significantly enhance the bearing capacity of the wall. Specifically, the peak load increases by 27% for RS1 and 98% for RS2 compared to the unreinforced wall. Nevertheless, the pushover curves of the reinforced structures exhibit distinct trends. Indeed, the RS1 curve shows a notable nonlinear behavior up to the peak load, followed by a softening branch that converges with the softening curve of the unreinforced wall as the control displacement (δ) increases. Conversely, the RS2 curve demonstrates a significant rise in bearing capacity up to a horizontal displacement of approximately 6.5 mm, followed by a sharp reduction. Indeed, the curve presents a series of sudden drops denoting the complete loss of the bearing capacity.

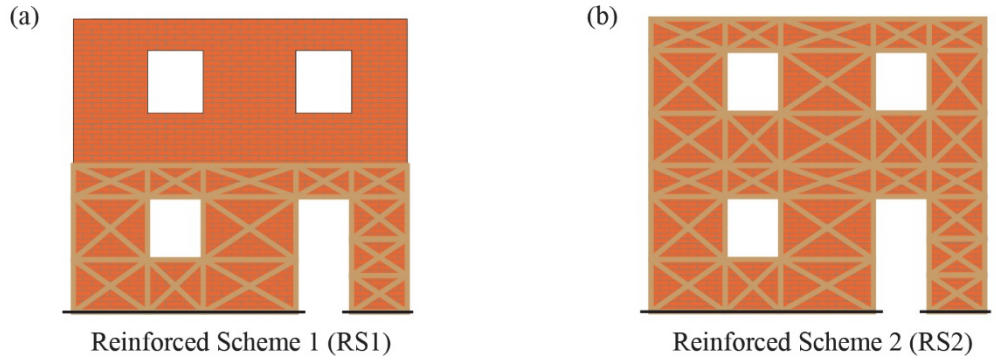

Figure 14: A two-story masonry wall: (a) Reinforced scheme 1 (RS1); (b) Reinforced scheme 2 (RS2).

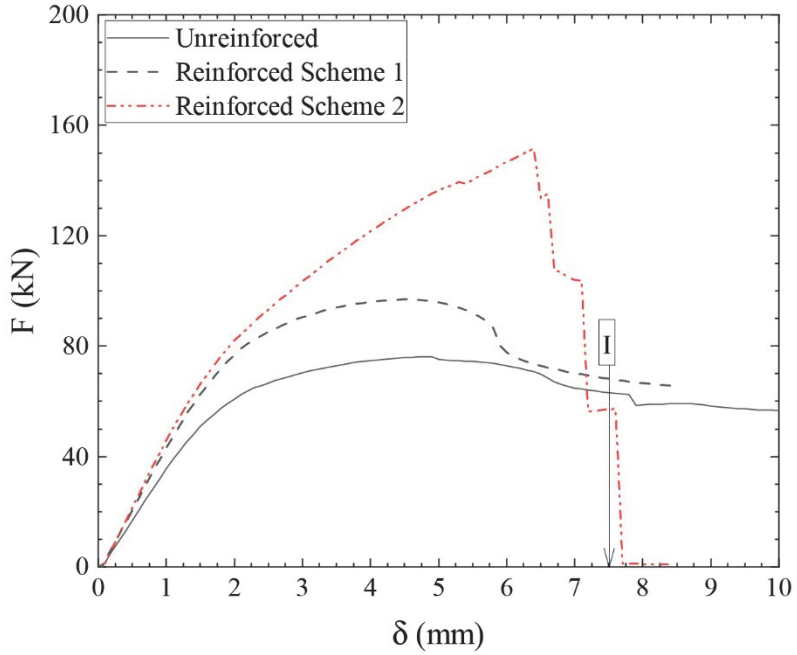

Figure 15: A two-story masonry wall: Pushover curves and effect of the reinforced schemes.

To analyze the mechanical behavior of the walls in detail, Fig. 16-a and b present the damage map of the interface elements and snapshots of the deformed wall configuration for the horizontal displacement value marked by the Roman numeral I in Fig. 15, respectively. In particular, in the damage map of interface elements (Fig. 16-a), regions of tensile failure are marked in red, while areas of compressive failure are marked in blue. For the timber frame retrofit system, damaged elements are marked in black, and undamaged elements are marked in brown.

The results for RS1 denote that the failure of the structure occurs because of the progressive failure of the unreinforced portion of the wall (*i.e.*, the upper level). As expected, comparing the damage maps of the unreinforced wall and that of RS1 reveals that reinforcing the bottom level of the wall shifts the occurrence of failure mechanisms to the upper level.

In this scenario, the masonry fails due to diagonal shear failure mechanisms in the left-upper and bottom-right regions, while the timber frame remains undamaged. Specifically, examining the damage map of the bottom-right pier shows that the refined timber frame scheme has significantly reduced the amount of damage.

On the other hand, the results for RS2 denote that the crisis of the wall occurs because of the breakage of two diagonal bracing members of the lower level, specifically the ones placed to the left and the central bottom piers. Such breakages involve the failure of the corresponding portion of the masonry. In particular, the left and central piers fail due to sliding (bond failure) and diagonal shear failure mechanisms, respectively. It is worth noting that the presence of the timber frame retrofitting system in the bottom wall alters the damage typology. Nevertheless, the proposed retrofit system determines an increment of the bearing capacity of the wall in both cases, thus highlighting its beneficial effect.

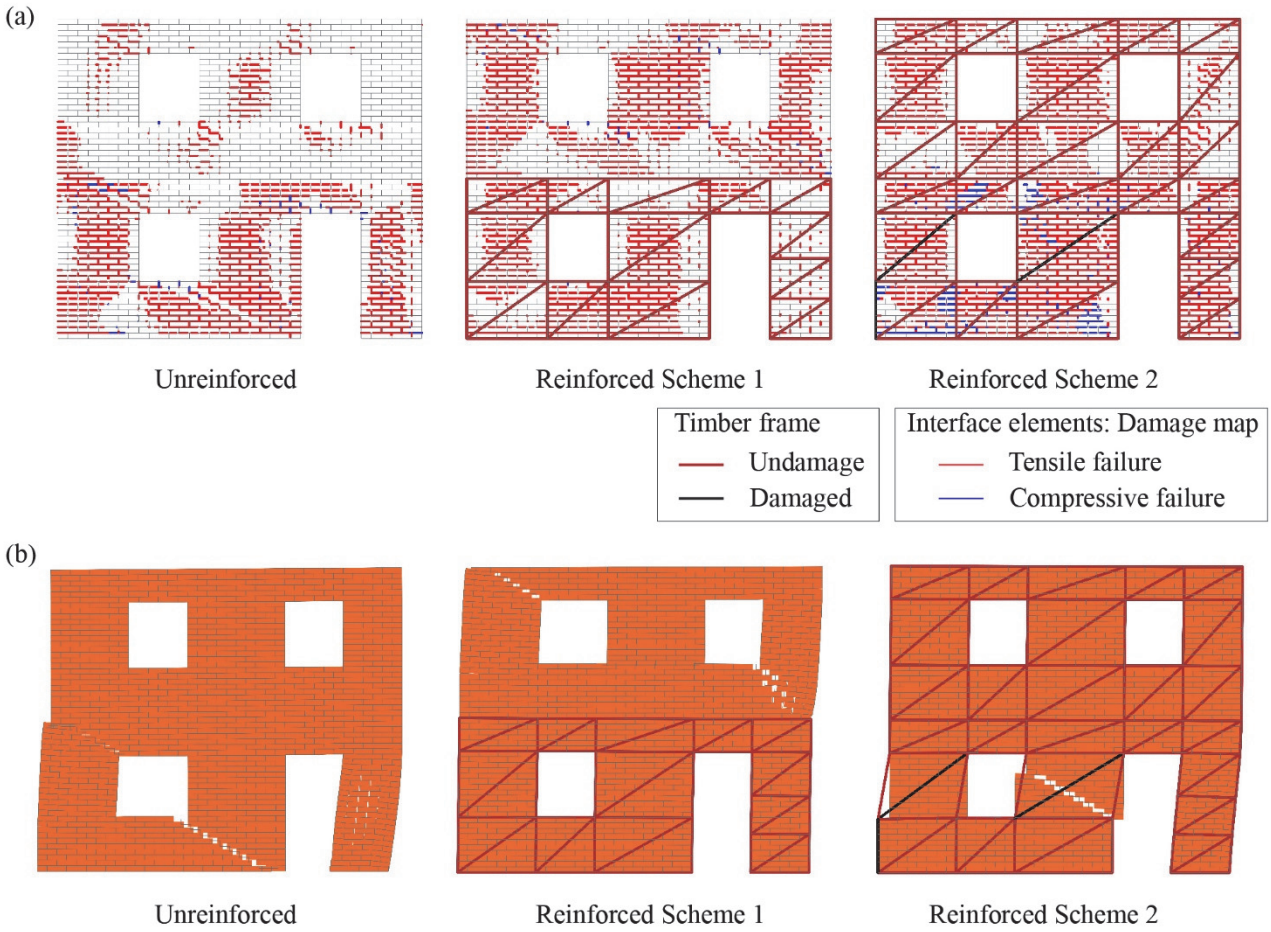

Figure 16: A two-story masonry wall: (a) Map of the damage inside interface elements (b) Snapshots of the deformed configurations of the masonry wall relative to the horizontal displacement values marked by Roman numerals in Fig. 15-b.

CONCLUSIONS

This paper proposes a refined FE-based modeling strategy for reproducing the failure behavior of periodic masonry structures reinforced via external timber-based retrofit solutions. The proposed model offers a detailed schematization of the masonry. Specifically, the brick units are modeled by two-dimensional linear elastic elements, while mortar joints are implicitly accounted for by means of zero-thickness cohesive interface elements, which efficiently reproduce the nonlinear behavior of masonry because of the occurrence of failure mechanisms of the mortar joints. Reinforced timber frame elements are modeled using truss elements experiencing elastic brittle fracture behavior.

The proposed study has been developed with the aim of achieving twofold goals: (*i*) proposing a refined modeling strategy for accurately reproducing the failure behavior of unreinforced periodic masonry structures and (*ii*) assessing the efficacy of timber frame structures as an external reinforcement technique to enhance the bearing capacity of the masonry against lateral actions. To this end, two case studies were analyzed: a masonry panel with an opening subjected to shear force and a two-story masonry wall, similar to those present in real-life masonry buildings, investigated by means of pushover analyses. The results demonstrated that the proposed model accurately replicates the failure behavior of the unreinforced masonry. Indeed, the load-displacement curve obtained from the proposed numerical model shows excellent agreement with both experimental and numerical data available in the literature.

Besides, the results highlight the benefits offered by the proposed retrofitting technique based on the use of timber frame structures as external reinforcement for the unreinforced masonry. In fact, the results showed that the retrofitting system significantly enhances the bearing capacity of the masonry against lateral loads. However, the results revealed that the use of the proposed retrofitting system can configure brittle behavior in reinforced masonry under failure. The analysis of different retrofitting schemes revealed that the configuration of the timber frame is crucial to avoid brittle failure

mechanisms. The optimal configuration should prevent the simultaneous failure of multiple components of the retrofitting structures, thereby distributing the stresses more evenly.
In summary, the proposed retrofitting strategy has proven effective in enhancing the load-bearing capacity of masonry structures. However, the timber frame configuration must be carefully designed to avoid sudden failures and ensure a more ductile structural behavior. Further research should be conducted to identify better configurations of the timber-frame retrofitting system that are able to mitigate the brittle behavior experienced by the reinforced masonry once that some bracing elements fail. In this line, it would be interesting to define a detailed numerical model capable of reproducing the behavior of joint connections between the timber frame components. This would enable the design of proper joint connections that can increase the ductility of the timber-frame sub-structure. Alternatively, one could explore the response of highly redundant timber frame retrofitting systems (*i.e.*, structures composed of many bracing elements).

ACKNOWLEDGMENTS

This article is supported by the Ministry of University and Research (MUR) as part of the FSE REACT-EU - PON 2014-2020 "Research and Innovation" resources – Green Action - DM MUR 1062/2021 - Title of the Research: "Advanced models and sustainable strategies for reduction of the risk of historical-cultural buildings".
Arturo Pascuzzo, who worked on the project mentioned above until January 31, 2024, gratefully acknowledges the financial support of the Ministry of University and Research (MUR) as part of the FSE REACT-EU - PON 2014-2020 "Research and Innovation" resources – Green Action - DM MUR 1062/2021 and sincerely thanks Maletta Ercole S.R.L. and its CEO, Angela Therese Maletta, for their invaluable support and assistance throughout this work.

REFERENCES

[1] Lourenco, P. (1996). Computational Strategy for Masonry Structures.
[2] Almssad, A., Almusaed, A., Homod, R.Z. (2022). Masonry in the Context of Sustainable Buildings: A Review of the Brick Role in Architecture, Sustainability, 14(22), p. 14734. DOI: 10.3390/su142214734.
[3] Debnath, P., Halder, L., Chandra Dutta, S. (2022). Damage survey and seismic vulnerability assessment of unreinforced masonry structures in low-intensity Ambasa earthquake of northeast India, Structures, 44, pp. 372–388. DOI: 10.1016/j.istruc.2022.08.005.
[4] Zhang, Y., Wang, Z., Jiang, L., Skalomenos, K., Zhang, D. (2023). Seismic fragility analysis of masonry structures considering the effect of mainshock-aftershock sequences, Engineering Structures, 275, p. 115287. DOI: 10.1016/j.engstruct.2022.115287.
[5] D'Altri, A.M., Sarhosis, V., Milani, G., Rots, J., Cattari, S., Lagomarsino, S., Sacco, E., Tralli, A., Castellazzi, G., de Miranda, S. (2020). Modeling Strategies for the Computational Analysis of Unreinforced Masonry Structures: Review and Classification, Arch Computat Methods Eng, 27(4), pp. 1153–1185. DOI: 10.1007/s11831-019-09351-x.
[6] Vandoren, B., De Proft, K., Simone, A., Sluys, L.J. (2013). Mesoscopic modelling of masonry using weak and strong discontinuities, Computer Methods in Applied Mechanics and Engineering, 255, pp. 167–182. DOI: 10.1016/j.cma.2012.11.005.
[7] Dugdale, D.S. (1960). Yielding of steel sheets containing slits, Journal of the Mechanics and Physics of Solids, 8(2), pp. 100–104. DOI: 10.1016/0022-5096(60)90013-2.
[8] Kármán, Th., Kuerti, G., van den Dungen, F.H., Howarth, L. eds., Advances in Applied Mechanics, 7, pp. 55–129.
[9] Greco, F., Leonetti, L., Lonetti, P. (2015). A novel approach based on ALE and delamination fracture mechanics for multilayered composite beams, Composites Part B: Engineering, 78, pp. 447–458. DOI: 10.1016/j.compositesb.2015.04.004.
[10] Pepe, M., Pingaro, M., Trovalusci, P., Reccia, E., Leonetti, L. (2020). Micromodels for the in-plane failure analysis of masonry walls: Limit Analysis, FEM and FEM/DEM approaches, Frattura Ed Integrità Strutturale, 14(51), pp. 504–516. DOI: 10.3221/IGF-ESIS.51.38.
[11] Gaetano, D., Greco, F., Leonetti, L., Lonetti, P., Pascuzzo, A., Ronchei, C. (2022). An interface-based detailed micro-model for the failure simulation of masonry structures, Engineering Failure Analysis, 142, p. 106753. DOI: 10.1016/j.engfailanal.2022.106753.

[12] Gaetano, D., Greco, F., Leonetti, L., Pascuzzo, A., Skrame, A. (2022). Comparative finite element modelling approaches for the seismic vulnerability analysis of historical masonry structures: the case study of the Cathedral of Catanzaro (Italy), International Journal of Masonry Research and Innovation, 7(6), pp. 600–623. DOI: 10.1504/IJMRI.2022.126544.
[13] Greco, F., Gaetano, D., Leonetti, L., Lonetti, P., Pascuzzo, A., Skrame, A. (2022). Structural and seismic vulnerability assessment of the Santa Maria Assunta Cathedral in Catanzaro (Italy): classical and advanced approaches for the analysis of local and global failure mechanisms, Frattura Ed Integrità Strutturale, 16(60), pp. 464–487. DOI: 10.3221/IGF-ESIS.60.32.
[14] Yavartanoo, F., Kang, T.H.-K. (2022). Retrofitting of unreinforced masonry structures and considerations for heritage-sensitive constructions, Journal of Building Engineering, 49, p. 103993. DOI: 10.1016/j.jobe.2022.103993.
[15] Corradi, M., Mustafaraj, E., Speranzini, E. (2023). Sustainability considerations in remediation, retrofit, and seismic upgrading of historic masonry structures, Environ Sci Pollut Res, 30(10), pp. 25274–25286. DOI: 10.1007/s11356-021-17490-7.
[16] Damiani, N., Guerrini, G., Graziotti, F. (2024). Design procedure for a timber-based seismic retrofit applied to masonry buildings, Engineering Structures, 301, p. 116991. DOI: 10.1016/j.engstruct.2023.116991.
[17] Guerrini, G., Damiani, N., Miglietta, M., Graziotti, F. (2024). Experimental validation of analytical equations for retrofitting masonry buildings with timber frames and boards, Engineering Structures, 300, p. 117124. DOI: 10.1016/j.engstruct.2023.117124.
[18] Guerrini, G., Damiani, N., Miglietta, M., Graziotti, F. (2023). Numerical simulation of a timber retrofit solution for unreinforced masonry buildings, Procedia Structural Integrity, 44, pp. 1877–1884. DOI: 10.1016/j.prostr.2023.01.240.
[19] Lagomarsino, S., Penna, A., Galasco, A., Cattari, S. (2013). TREMURI program: An equivalent frame model for the nonlinear seismic analysis of masonry buildings, Engineering Structures, 56, pp. 1787–1799. DOI: 10.1016/j.engstruct.2013.08.002.
[20] Efficiency and Seismic Behaviour of Existing Masonry Buildings, Sustainability, 13(18), p. 10379. DOI: 10.3390/su131810379.
[21] Le Minh, H.-., Khatir, S., Abdel Wahab, M., Cuong-Le, T. (2021). A concrete damage plasticity model for predicting the effects of compressive high-strength concrete under static and dynamic loads, Journal of Building Engineering, 44, p. 103239. DOI: 10.1016/j.jobe.2021.103239.
[22] Vermeltfoort, A.T., Raijmakers, T., Janssen, H.J.M. (1993). Shear tests on masonry walls., 6th North American Masonry Conference, Philadelphia, Pennsylvania, USA.
[23] Lourenço, P.B., Rots, J.G. (1997). Multisurface Interface Model for Analysis of Masonry Structures, Journal of Engineering Mechanics, 123(7), pp. 660–668. DOI: 10.1061/(ASCE)0733-9399(1997)123:7(660).
[24] Maria D'Altri, A., Lo Presti, N., Grillanda, N., Castellazzi, G., de Miranda, S., Milani, G. (2021). A two-step automated procedure based on adaptive limit and pushover analyses for the seismic assessment of masonry structures, Computers & Structures, 252, p. 106561. DOI: 10.1016/j.compstruc.2021.106561.
[25] Milani, G. (2011). Simple homogenization model for the nonlinear analysis of in-plane loaded masonry walls, Computers & Structures, 89(17), pp. 1586–1601. DOI: 10.1016/j.compstruc.2011.05.004.